

# Oscillations of the intertropical convergence zone and the genesis of easterly waves. Part I: diagnostics and theory

Violeta E. Toma · Peter J. Webster

Received: 19 November 2008 / Accepted: 21 April 2009 / Published online: 13 May 2009  
© Springer-Verlag 2009

**Abstract** We examine the mean and transient state of the intertropical convergence zone (ITCZ) by analyzing data and using simple theory. We concentrate on the tropical eastern Pacific Ocean noting that there exists in this region a well-developed mean ITCZ. Furthermore, it is a region where there has been considerable discussion in the literature of whether easterly waves develop in situ or propagate westwards from the Atlantic Ocean. The region is typical of tropical regions where there is a strong cross-equatorial pressure gradient (CEPG): mean convection well removed from the equator but located equatorward of the maximum sea-surface temperature (SST) and minimum sea level pressure (MSLP). Further to the west, near the dateline where the CEPG is much smaller, convection is weaker and collocated with SST and MSLP extrema. It is argued that in regions of significant CEPG that the near-equatorial tropical system is inertially unstable and that the rectification of the instability for a given CEPG determines the location and intensity of the climatological ITCZ. Using simple theoretical arguments, we develop an expression for the mean latitude of the ITCZ as a function of the CEPG. We note on a day-by-day basis that the ITCZ is highly transient state with variability occurring on 3–8 day time scales. Transients with amplitudes about half of the mean ITCZ, propagate northwards from the near-equatorial southern hemisphere as anomalous meridional oscillations, eventually amplifying convection in the vicinity of the mean ITCZ. It is argued that in these longitudes of strong CEPG

the mean ITCZ is continually inertially unstable with advectons of anticyclonic vorticity across the equator resulting in the creation of an oscillating divergence–convergence doublet. The low-level convergence produces convection and the resultant vortex tube stretching generates cyclonic vorticity which counteracts the northward advection of anticyclonic vorticity. During a cycle, the mid-troposphere heating near 10°N oscillates between 6 and 12 K/day at the inertial frequency of the latitude of the mean convection. As a result, there exists an anomalous and shallower, oscillating meridional circulation with a magnitude about 50% of the mean ITCZ associated with the stable state following the generation of anticyclonic vorticity. Further, it is argued that the instabilities of the ITCZ are directly associated with in situ development of easterly waves which occur with the inertial period of the latitude of the mean ITCZ. The dynamical sequences and the genesis of easterly waves are absent in the regions further to the east where the CEPG is much weaker or absent altogether. In a companion study (Part II), numerical experiments are conducted to test the hypothesis raised in the present study.

**Keywords** Intertropical convergence zone · Mean and transient tropical convection · Genesis of easterly waves · Inertial instability · Cross-equatorial pressure gradient

## 1 Introduction

The climatological intertropical convergence zone (ITCZ) may be thought as of a band of deep convection at the confluence of the northeast and southeast trade wind. The ITCZ, so defined, follows a distinct annual cycle located in the summer hemisphere in most tropical locations, lagging

---

V. E. Toma · P. J. Webster (✉)  
School of Earth and Atmospheric Sciences,  
Georgia Institute of Technology, Atlanta, GA, USA  
e-mail: pjw@eas.gatech.edu

V. E. Toma  
e-mail: vtoma@eas.gatech.edu

in latitude behind the maximum in solar radiation by about two months. The eastern equatorial Pacific Ocean is an exceptional region where the ITCZ remains in the northern hemisphere throughout the entire year except during El Niño periods. Small deviations in the climatological location of the ITCZ are thought to produce surpluses or deficits of precipitation in the West African Sahel (Grist and Nicholson 2001), northeastern Brazil (Biasutti et al. 2003) and other regions throughout the tropics.

Figure 1a shows the mean spatial characteristics of tropical Pacific Ocean convection for June, July and August (JJA) for the non-El Niño year of 1996. Out-going long-wave radiation (OLR) is used as a proxy for convection. We have chosen the tropical eastern Pacific Ocean as a primary focus area because there exists a well defined mean ITCZ. In addition, it is a region about which there has been strong debate of whether the convective waves found eastern Pacific develop in situ (e.g., Ferreira and Schubert 1997; Serra et al. 2008) or propagate westwards from the Atlantic Ocean (e.g., Frank 1970; Raymond et al. 2006). The deepest convection lies east of 120°W across a broad region from about 5°N to the Central American and Mexican coasts. The convective maximum extends westward and narrowing in latitudinal extent before merging with a much broader and less intense region of convection to the west of 170°E.

Figure 1b and c shows the mean distributions of sea-surface temperature (SST) and mean sea-level pressure (MSLP) in the tropical Pacific domain. The western Pacific is dominated by a large expanse of warm and relatively low salinity water extending broadly across the equator. This area with generally enhanced convection is referred to as the tropical Pacific warm pool (e.g., Webster and Lukas 1992). A second Pacific warm pool is found east of 120°W and north of 12–15°N off Mexico and Central America. The MSLP field (Fig. 1c) follows the SST distribution with high pressure overlying cool SST (e.g., southeastern Pacific Ocean) and low pressure associated with higher SSTs (e.g., the western equatorial and the tropical northeastern Pacific Ocean).

Figure 1 also shows that in certain regions that the ITCZ is located equatorward of the maximum SST and minimum MSLP, as noted earlier by Ramage (1974); Sadler (1975); Hastenrath and Lamb (1977a, b); Waliser and Somerville (1994) and Tomas and Webster (1997); henceforth referred to as TW). In other regions such as the western Pacific, there is a closer relationship between the ITCZ and maximum SST. Figure 2 shows latitudinal distributions of SST, MSLP, OLR and the 850 hPa absolute vorticity ( $\eta = f + \zeta$  where  $f$  is the Coriolis force and  $\zeta$  the vertical component of relative vorticity) averaged across two longitude bands that show contrasting relationships. The first band cuts across the ITCZ in the eastern Pacific (section A in Fig. 1a, between 120° and 110°W) whilst the second band bisects

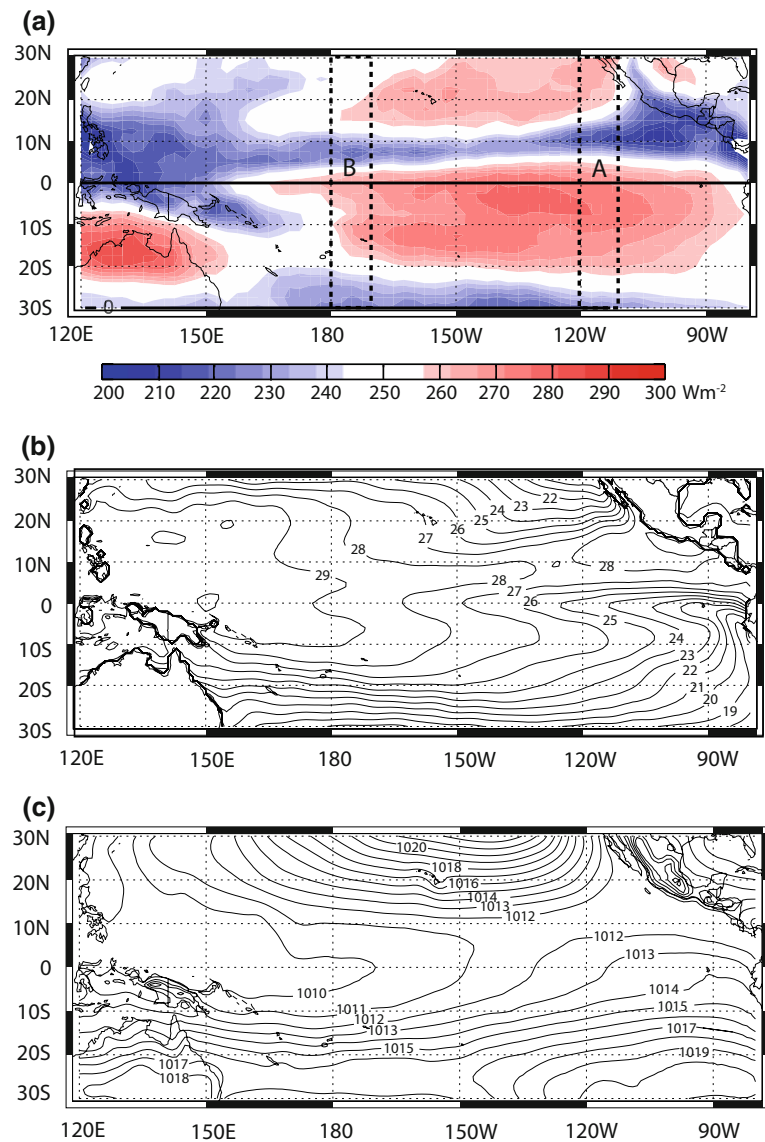
the broader central Pacific ITCZ (section B between 180° and 170°W). In section A, the OLR minimum is found at 9°N, while the SST maximum and MSLP minimum lie at 12°N and 13°N, respectively. Similar relationships between SST, MSLP and OLR are also found around the tropics where the cross-equatorial pressure gradient (CEPG) is large (TW, Nicholson and Webster 2007). In section B, there are very different relationships between convection and SST and MSLP. For example, there are two SST maxima; one at 5°N and the other at 6°S and the MSLP minimum resides at 2°S. The OLR minimum is centered further poleward at 8°N. These observations are consistent with the conclusions of Lindzen and Nigam (1987) that SST gradients are important in determining the location of convection. In the eastern Pacific, the strongest gradient is cross-equatorial and latitudinal. In the western Pacific, where the SST is more homogeneous, the strongest gradient is longitudinal.

A number of studies have attempted to address the off-equatorial location of the mean ITCZ and the existence of the climatological ITCZ equatorward of the warmest SST and lowest MSLP. For example, Waliser and Somerville (1994) suggested that convection occurs 4°–12° away from the equator because, at these latitudes, low-level convergence of moist air is optimized. TW (and later Tomas et al. 1999, hereafter THW) noted the importance of the magnitude of the CEPG in determining the location of the ITCZ. A statistically significant negative correlation was found between the magnitude of the CEPG and the latitude of the zero absolute vorticity contour ( $\eta = 0$ ). It was argued that a finite CEPG produces an incursion of either anticyclonic vorticity into the northern hemisphere or cyclonic vorticity into the southern hemisphere. Both of these situations are inertially unstable (e.g., Stevens 1983, TW). THW noted that although the mean cross-equatorial flow and the location of convection appeared to be consistent with inertial instability, the linear stability criterion was not met in regions of strong CEPG. But, as will be discussed later, this conclusion resulted from an assumption of greater atmospheric stability than is found in reality and, with more realistic values, the linear criterion is met.

TW noted a further peculiarity of the off-equator ITCZ. Rather than a meridional circulation occupying the entire troposphere, there appeared in the mean a secondary and weaker circulation restricted to the lower half of the troposphere. In a study of the eastern Pacific Ocean, Zhang et al. (2004) described this second cell in detail. We refer to this as the ZMB circulation. Considerable attention will be given to describing this cell in Sects. 4 and 5 as it proves to be indicative of transient processes within the mean ITCZ.

Viewed on a day-to-day basis, the ITCZ assumes a very different form than the mean state described above. Figure 3a shows daily OLR time series at two locations:

**Fig. 1** **a** Mean OLR distribution ( $\text{Wm}^{-2}$ ) over the Pacific Ocean for the period June–August, 1996. **b** Mean sea-surface temperature (SST  $^{\circ}\text{C}$ ) distribution across the Pacific Ocean. **c** Mean sea-level pressure (MSLP hPa)



$120^{\circ}\text{W}$ – $10^{\circ}\text{N}$  and  $180^{\circ}\text{W}$ – $10^{\circ}\text{N}$ , for the 10-year period 1991–2000. High frequency variance is evident in both sections with OLR with a  $200 \text{ Wm}^{-2}$  amplitude range signifying 3–8 day oscillations between convective and less-convective periods. Figure 3b shows daily OLR values along  $10^{\circ}\text{N}$  during a period in 1996. A general westward propagation is evident. These “easterly waves” (i.e., waves in the easterly wind regime) were described initially by Riehl (1945); Palmer (1952); Yanai et al. (1968); Chang (1970). Holton et al. (1971) suggested that the waves are fundamental building blocks of the mean ITCZ. During summer, in both the Pacific and Atlantic oceans, there are about 6–8 easterly waves per month. Figure 3c shows a spectral analysis of the OLR time series from 1981 to 2000 for the two longitudinal bands A and B. A high amplitude and broad peak in the 3–8 day range dominates the high frequency end of the spectra.

For later reference, values of the local inertial period ( $\omega_i = 2\pi/|f|$ ) are also plotted.

There have been a number of studies aimed at explaining the existence and character of easterly waves. Bates (1970) considered these waves to be basic instabilities of a zonally symmetric ITCZ in accord with Holton et al. (1971). Burpee (1972) proposed that easterly waves were generated over Africa as instabilities of an easterly jet formed by off-equator elevated heating of the African highlands. Thorncroft and Hoskins (1994) generalized the Burpee theory concluding that waves were formed from a joint barotropic–baroclinic instability of the African easterly jet stream. Easterly waves in the eastern Pacific Ocean were generally explained as waves propagating out of the Atlantic across Central America (e.g., Frank 1970), a perception that appears to have become generally accepted (e.g., Raymond et al. 2006). Zehnder et al. 1999 and Farlan

and Zehnder (1997) have suggested that the Sierra Madre, lying about 2,000 km north of the equator and the mountains of Central America to the east and northeast of the eastern Pacific warm pool lead to a barotropic instability and the genesis of tropical disturbances. Each of these studies considered the primary source of disturbances to be the Atlantic Ocean.

A recent study provides evidence for a different interpretation of the source of eastern Pacific easterly waves. Serra et al. (2008) find the formation and the character of the Pacific waves to be quite different from their Atlantic counterpart suggesting that the majority of Pacific waves were created in situ. A more recent study (Serra et al. 2009<sup>1</sup>) shows that only 4–8% of waves observed in the eastern Pacific Ocean cross Central America from the Atlantic. A specific mechanism for in situ development was not suggested. Earlier studies have argued that regional instabilities are the cause of easterly waves. For example, Ferreira and Schubert (1997) noted that the ITCZ becomes disturbed and that tropical cyclones form on the poleward side of the maximum convection. They argued that a baroclinic/barotropic instability caused the breakdown of the ITCZ. Wang and Magnusdottir (2005) suggested that the breakdown of the ITCZ was the result of convective heating-induced potential vorticity anomalies. Both of these studies assumed a preexisting ITCZ with neither presenting a physical explanation for the assumed location. Contrary to Fig. 2, Ferreira and Schubert assumed that  $\eta > 0$  in the northern hemisphere therefore asserting that the system was inertially stable.

There are a number of fundamental questions about the structure and maintenance of the ITCZ and easterly waves:

1. What processes determine the location and intensity of the mean ITCZ? Why does it change its character westwards across the Pacific Ocean with deeper convection in the east than in the west?
2. Is the shallow ZMB circulation a persistent feature of mean ITCZ or an artifact of sampling a transient oscillation of the ITCZ from one state to another?
3. Are there coherent high frequency oscillations of the mean ITCZ? If they occur, are they regional? Is the shallow ZMB circulation associated with these oscillations?
4. Is there a relationship between oscillations of the ITCZ and the generation of easterly waves observed in the tropics? Are easterly waves the result of regional

<sup>1</sup> An earlier version of this study exists: “Tracking tropical easterly waves across Central America and Mexico”, Y. Serra, Assoc. Research Prof. Department of Atmospheric Sciences, University of Arizona Climate Prediction Program for the Americas Principal Investigator meeting Silver Spring, MD 9/29–10/1/2008.

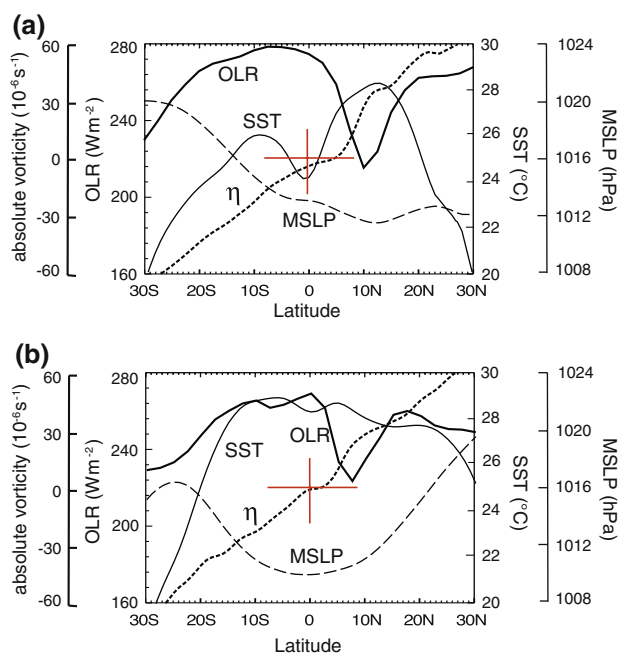


**Fig. 2** Cross-sections of OLR ( $\text{Wm}^{-2}$ ), SST ( $^{\circ}\text{C}$ ), MSLP (hPa) and absolute vorticity at 850 hPa ( $10^{-6} \text{ s}^{-1}$ ) defined in the text for the two longitudinal bands (a)  $120^{\circ}\text{W}$ – $110^{\circ}\text{W}$  and (b)  $180^{\circ}\text{W}$ – $170^{\circ}\text{W}$ , depicted as sections A and B in Fig. 1a. The red “cross-hairs” identify the location of  $\eta = 0$  and the equator

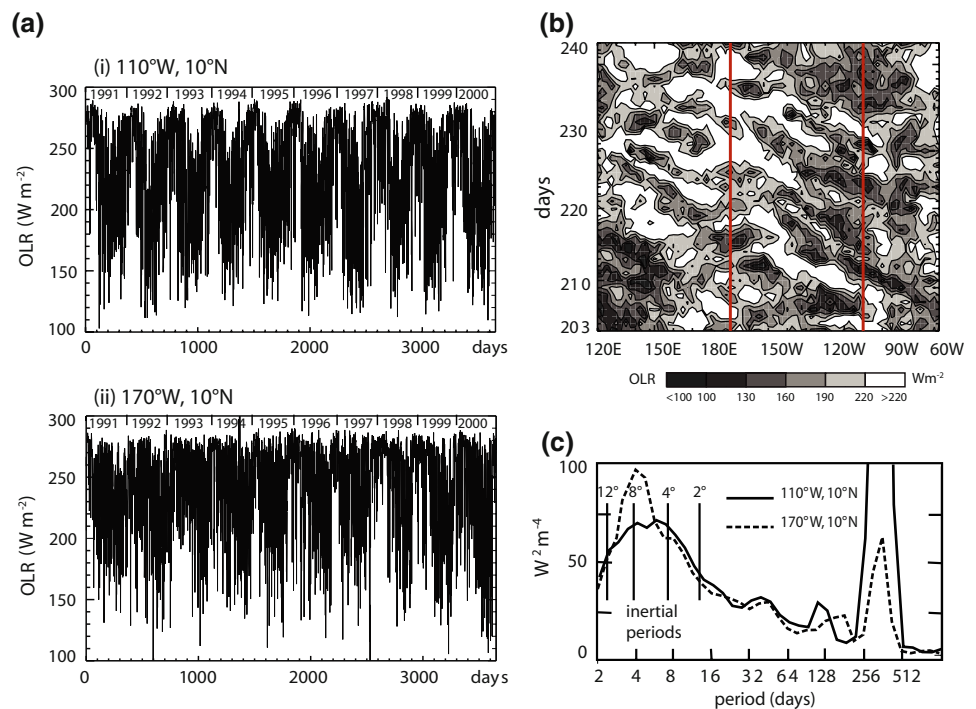
instabilities or are they generated remotely (e.g., Africa or higher latitudes)?

We will attempt to provide answers to these questions using a combination of theory, analyses and numerical experiments, the latter described. In the next section, the data used in the study will be described in a companion paper (Toma and Webster 2008, hereafter referred to as Part II). Section 3 discusses the structure of the mean ITCZ. Section 4 describes the transient nature of the ITCZ. Dynamical balances that occur in both the mean and during oscillations of the ITCZ are discussed in Sect. 5. A comprehensive set of experiments is described conclusions and summary are presented in Sect. 6.

## 2 Data

We choose the European Center for Medium Range Weather Forecasts (ECMWF) ERA-40 reanalysis data (Uppala et al. 2005) as the basic data set. ERA-40 has a  $1^{\circ} \times 1^{\circ}$  horizontal resolution and 18 levels in the vertical. The SST fields are derived from the weekly NOAA/NCEP (Reynolds et al. 2002) and OLR is used as a surrogate for convection. Long-term means were calculated over the period 1981–2000. Beyond the phenomenological reasons described above, the eastern Pacific Ocean was chosen because it was also the location of the East Pacific

**Fig. 3** **a** Time section of daily OLR ( $\text{Wm}^{-2}$ ) for the 10-year-period 1991–2000 at two locations *i* 120°W and *ii* 170°W along 10°N. Both locations exhibit high amplitude subseasonal oscillations: **b** time-longitude section of OLR ( $\text{Wm}^{-2}$ ) along 10°N between 120°E and 60°W. Contours are shown for 220, 190, 160, 130 and 100  $\text{Wm}^{-2}$ . The longitudinal domain is the same as in the panels of Fig. 1 and **c** Power spectra of OLR at two locations: 110°W–100°W (*solid line*) and 180°W–170°W at 10°N (*dashed line*)



Investigation of Climate experiment (EPIC: Raymond et al. 2004). The field phases of EPIC collected high resolution and quality data of the ocean and the atmosphere. We make use of some of the EPIC vertical atmospheric sounding data in the appendix.<sup>2</sup>

### 3 Character of the mean ITCZ

The upper panel of Fig. 4a shows the mean JJA meridional circulation for the period 1981–2000 for the strong CEPG section A (see Fig. 1a) in terms of mass streamfunction,  $\psi$ , derived by downward integration of the meridional mass flux. There is a broad band of rising motion located between 6°N and 12°N with subsidence to the south extending to 20°S and weak ascent to the north of the major convection. The major ascending region corresponds to a vertical incursion of moisture into the upper troposphere (shading). The lower panel shows the horizontal divergence field (contours) and the meridional wind component (shading). There is a layer of boundary layer cross-equatorial winds of magnitude  $>6 \text{ ms}^{-1}$  with a return flow aloft with speeds exceeding  $8 \text{ ms}^{-1}$ . A second weaker southward  $2 \text{ ms}^{-1}$  meridional velocity maximum occurs between 700 and 600 hPa also over the equator. This is the ZMB cell. In both panels, the zero absolute vorticity contour ( $\eta = 0$ : plotted as the bold dashed line) bisects the

meridional wind maximum in the lower troposphere. Equatorward of the zero contour the northward winds accelerate whilst, on the poleward side, there is a region of rapid deceleration corresponding in location to the rising arm of the meridional cell. The result is a boundary layer divergence–convergence doublet centered on the  $\eta = 0$  contour. In the upper troposphere there is a strong region of divergence located directly above the boundary layer convergence with strong southerly winds to the south and a southward displacement of the  $\eta = 0$  contour into the southern hemisphere.

Figure 4b is the counterpart of Fig. 4a except for section B (see Fig. 1a), 8,000 km to the west, located in a region of weak CEPG. A completely different meridional circulation structure is found. Near the equator, the magnitude of  $\psi$  has decreased by a factor of four. Instead of a strong cross-equatorial meridional circulation, the weak ascent is confined to the northern hemisphere collocated with the maximum SST. Boundary layer convergence is also weak and the  $\eta = 0$  contour is aligned with the equator throughout the troposphere. There is no evidence of a ZMB circulation in the central-western Pacific.

## 4 Transient states of the ITCZ

### 4.1 Character of the transients

Figure 5a and b shows latitude–time plots of OLR anomalies and the 925 hPa  $\eta$  averaged across the two sections A and B,

<sup>2</sup> EPIC data are accessible at [http://data.eol.ucar.edu/master\\_list/?project=EPIC](http://data.eol.ucar.edu/master_list/?project=EPIC).

**Fig. 4** Characteristics of the mean 1981–2000 summer (June–August) meridional circulation in the east Pacific Ocean averaged for **a** 120°W–110°W (section A) and **b** 170°W–180°W (section B). Panel *i* shows the mass streamfunction ( $10^{11} \text{ kg s}^{-1}$ ) and relative humidity (shading relative to bar below figure: %) *ii* horizontal wind divergence ( $10^{-6} \text{ s}^{-1}$  with red contours positive, black contours negative) and meridional wind (shaded contours  $\text{ms}^{-1}$ , bottom scale)

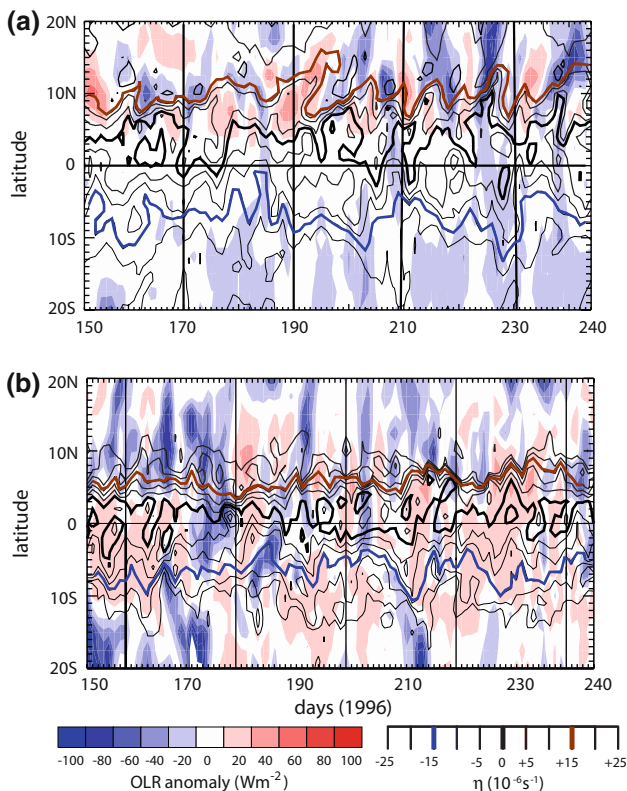
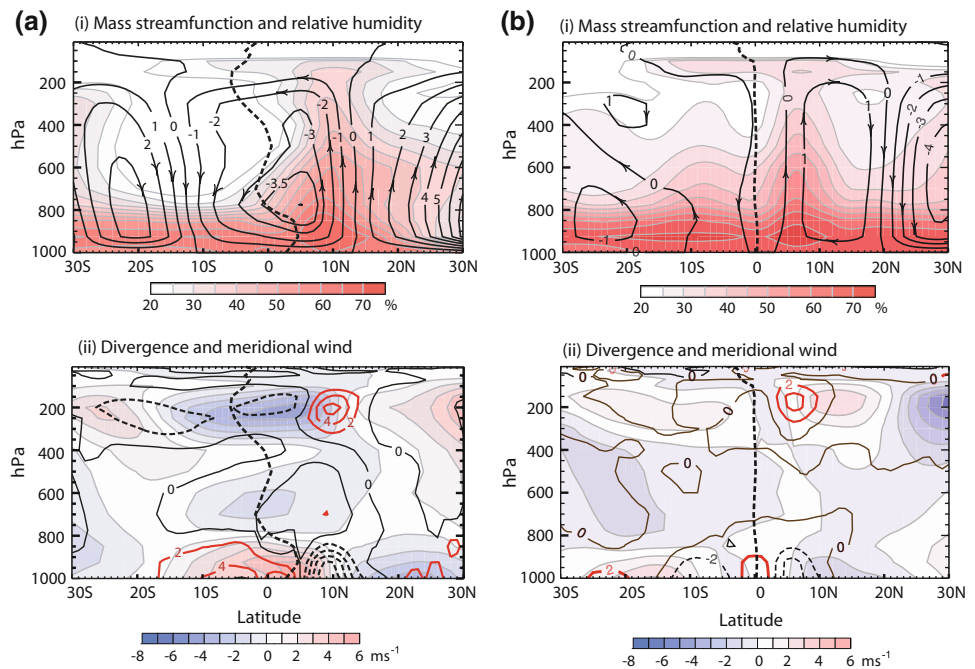


**Fig. 5** Time–latitude evolution of daily values of anomalous OLR (shaded, bottom scale  $\text{W m}^{-2}$ ) and absolute vorticity ( $\eta \text{ } 10^{-6} \text{ s}^{-1}$ ) at 925 hPa in the **a** 120°W–110°W (section A) longitude sector and **b** 180°W–170°W (section B) for periods in the northern hemisphere summer of 1996. Commencing and ending dates in the sections are May 29 (day 150) and August 27 (day 240) for 1996. Contours intervals of  $\eta$  are every  $5 \times 10^{-6} \text{ s}^{-1}$  between  $\pm 25 \times 10^{-6} \text{ s}^{-1}$ . Bold contours relative to bottom scale, show the  $\eta = +15$ , 0 and  $-15 \times 10^{-6} \text{ s}^{-1}$  contours

respectively. Periods of enhanced (negative OLR values: blue) and reduced convection (positive OLR: red) exist in both regions with changes in sign occurring every few days. In the eastern section, convective activity is confined between 5°N and 12°N. The convection in the western section, in contrast, appears less spatially restricted with convective events occurring on either side of the equator. There are also distinct differences in the absolute vorticity fields. The eastern section shows that the absolute vorticity is generally anticyclonic south of about 5°N but with large excursions of the zero contour both to the north of 5°N and towards the equator. North of the equator, the northward extent of the  $+15 \times 10^{-6} \text{ s}^{-1}$  contour (bold red) varies in both space and time. In the western section (Fig. 5ii), the variations of  $\eta$  are confined closer to the equator. The differences in the transient positions of the  $\eta = 0$  between the east and west sections can be seen in Fig. 2. The “cross-hairs” in the center of the diagrams denote the latitude of the equator and the  $\eta = 0$  contour. In the eastern section there is anticyclonic vorticity in the mean extending to at least 5°N, considerably further poleward than in the west.

To examine further the associations between convection and absolute vorticity, we take advantage of the strong high-frequency band apparent in the spectral analysis (Fig. 3c). Figure 6 shows a longitude–time section of OLR, similar to Fig. 3b, except for the 4–8 day period band. The filtered diagram shows strong westward propagation of OLR anomalies with magnitudes  $>50 \text{ W m}^{-2}$ , wavelengths of approximately 30°–40° longitude or 3,000–4,000 km and propagation speeds of 8–10  $\text{ms}^{-1}$  in the eastern Pacific similar to characteristics found by Serra et al. (2008).

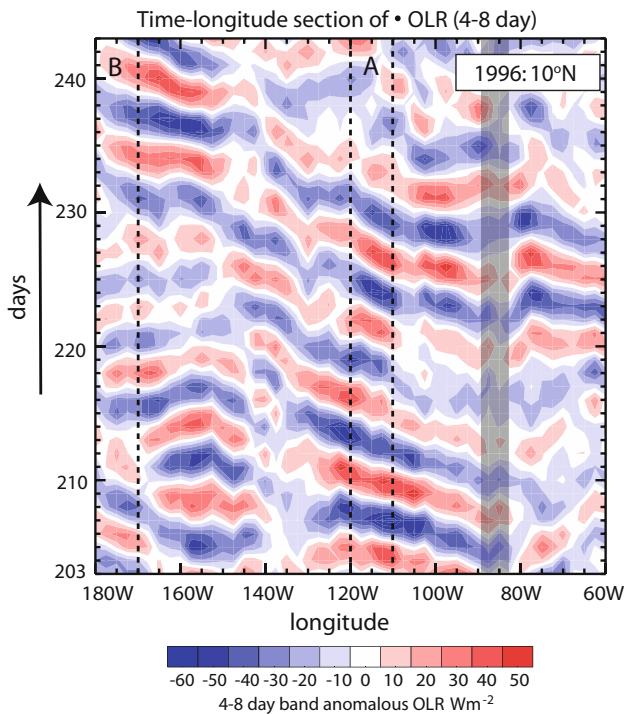


**Fig. 6** Longitude–time plot of OLR anomalies ( $\text{Wm}^{-2}$ ) in the eastern Pacific Ocean along  $10^\circ\text{N}$  between  $180^\circ$  and  $60^\circ\text{W}$ . The data has been filtered to emphasize the 4–8-day-period band. The shaded band indicates the land area separating the Gulf of Mexico to the east and the Pacific Ocean to the west. General westward propagation occurs throughout the domain but across the Isthmus of Panama, there appears to be a loss of phase indicating perhaps, that the Pacific Ocean disturbances may be generated locally and do not propagate from the Atlantic Ocean

Are the disturbances in Fig. 6 generated in situ or are they remnants of waves propagating across the Isthmus of Panama from the Atlantic? Between days 200 and 220, the waves in the Pacific appear to have no corresponding perturbations to the east of the Isthmus. Between days 220 and 230, waves are evident on the east side of the Isthmus but they appear to arrive 2–3 days earlier than would be necessary to explain Pacific waves by simple propagation. It is possible that a phase change occurs across the Isthmus but the processes that could account for such a change are unknown. After day 230 there is little evidence of waves to the east of the Isthmus although the region to the west is quite perturbed. Serra et al. (2008, 2009) note that some waves propagate from the Atlantic but found that most waves appeared to form in the eastern Pacific Ocean. The results presented here for 1996, corroborated by similar analyses for other years in the data set (not shown), appear to agree with Serra et al. conclusions.

Finally, the analysis of Fig. 5 was repeated but with the application of a 4–8 day band pass filter. These analyses are shown in Fig. 7. The uppermost panels show the band-passed OLR and 925 hPa  $\eta$ -fields while the lower two

panels show the band-passed divergence fields at 925 and 250 hPa. In the eastern section (Fig. 7a), OLR anomalies are negatively correlated with vorticity and show a tendency for northward propagation from south of the equator culminating in the region of maximum convection near  $10^\circ\text{N}$ . The low level divergence (panel ii) correlates negatively with convection and, in general, is out-of-phase with the 250 hPa divergence field (panel iii). The overall configuration of the fields suggests a systematic northward propagation of alternatively signed anomalies across the equator into the convective region of the mean ITCZ near  $10^\circ\text{N}$ . The distributions of  $\eta$  and  $\nabla \cdot V$  for the western section (Fig. 7b) are dramatically different to those further east. The magnitudes of all fields are smaller and there is less evidence of systematic association between OLR and absolute vorticity. The upper and lower level divergence patterns have a similar out-of-phase relationship but the extrema occur closer to the equator.

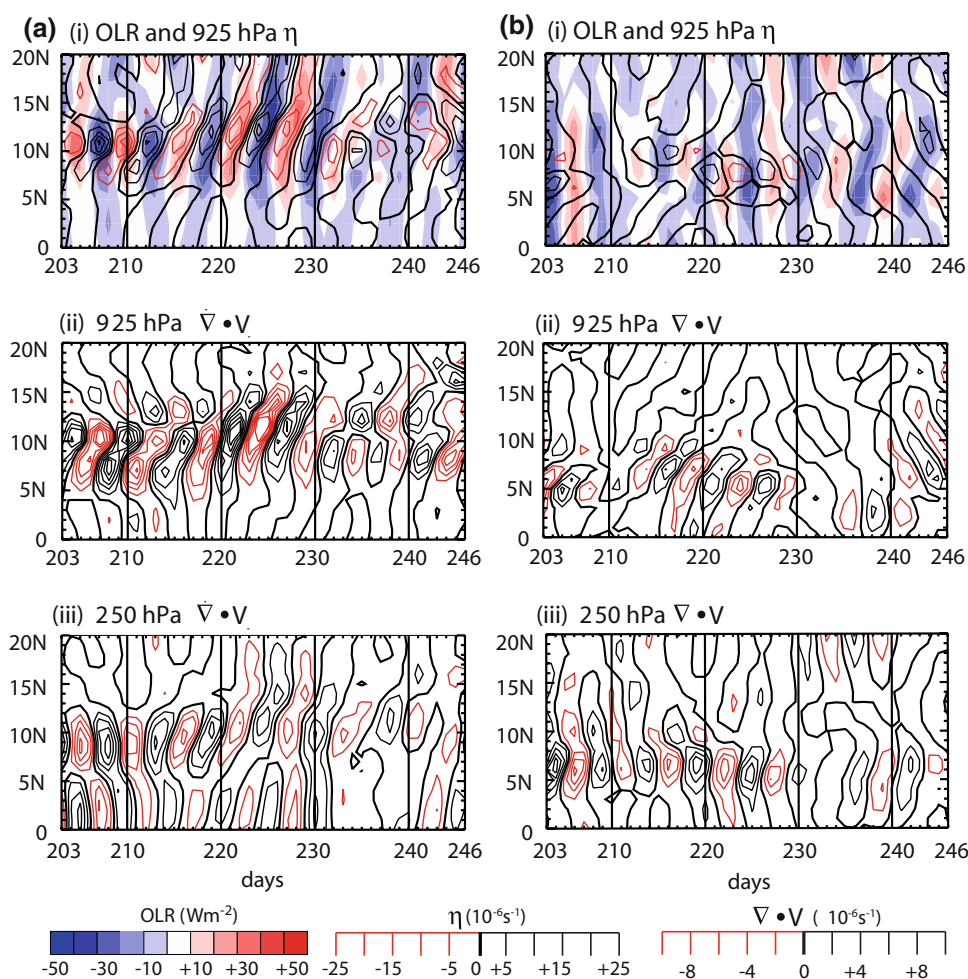
One could argue that the alternation of convection and vorticity is the result of the propagation of troughs and ridges past a point. But there is a complicating factor in that there appears to be a coherent poleward propagation from the near-equatorial southern hemisphere to latitudes poleward of  $10^\circ\text{N}$  taking roughly 4–6 days in transit. The question of in situ or remote origin of Pacific waves will be readdressed in the modeling study reported in Part II.

#### 4.2 Composite of the transients

Figure 7 suggests that there are two major extremes in the 4–8 day period band, one dominated by anticyclonic absolute vorticity ( $\Delta\eta < 0$ ) and shallow convection ( $\Delta\text{OLR} \gg 0$ ) and a second dominated by cyclonic absolute vorticity ( $\Delta\eta > 0$ ) and deep convection ( $\Delta\text{OLR} \ll 0$ ). Composites are constructed relative to a “day 0” defined by  $\Delta\text{OLR}$  values at  $7.5^\circ\text{N} > -20 \text{ Wm}^{-2}$ . During the period 1998–2000, 40 cases for section A were chosen. These were used to define states of the ITCZ at days  $-3, -2, \dots, +2, +3$  between  $30^\circ\text{S}$  and  $30^\circ\text{N}$ . In essence, the composite circulations, so defined, may be thought of as transient anomalies superimposed upon the long-term mean circulation shown in Fig. 4a. Disturbances that attained tropical cyclone intensity were not included in the composites.

Figure 8 shows the latitude–height structure of the composite meridional circulation from day  $-3$  to day  $+3$  with the long-term mean circulation excluded. The left-hand panels show the mass stream function ( $\psi$ ) and relative humidity (RH %) while the right-hand panels show the meridional wind speed ( $v \text{ ms}^{-1}$ ; shaded lower scale) and divergence ( $\nabla \cdot V$ :  $10^{-6} \text{ s}^{-1}$ , contours with zero line omitted for clarity). The first point to note is that changes in the circulation, throughout the composite period, extend

**Fig. 7** Time–latitude plots of the 4–8 day filtered data for a 44 day period during the summer of 1996 between the equator and 20°N for two bands **a** 110°W–100°W (section A) and **b** 180°W–170°W (section B). Panel *i* shows OLR anomalies ( $\Delta\text{OLR}$   $\text{Wm}^{-2}$ , shading lower scale) and anomalies in the absolute vorticity field ( $\Delta\eta$ :  $10^{-6} \text{ s}^{-1}$ , contours, lower scale). Bold black contour denotes  $\Delta\eta = 0$ . Panels *ii* and *iii* show divergence at 925 and 250 hPa, respectively, relative to the contour scale at the bottom of figure



over the entire 30°S–30°N latitudinal domain. The sequence may be described as follows.

#### 4.2.1 Day –3

A broad meridional circulation extends from 30°S to 10°N with subsidence from 10°S to 10°N collocated with boundary layer divergence. A negative mid-tropospheric relative humidity anomaly is located north of the equator. Upper tropospheric meridional winds converge near 10°N. Anomalous rising motion is apparent in the southern hemisphere and corresponds to the relatively weak negative anomalies in OLR.

#### 4.2.2 Day –2

A shallow cell has formed in the region between the equator and 10°N with weak rising motion to the north. Low tropospheric convergence has developed to the south of 10°N. Convergence still exists in the upper troposphere but a region of lower-middle tropospheric divergence with a southward flow accompanies the development of the shallow cell.

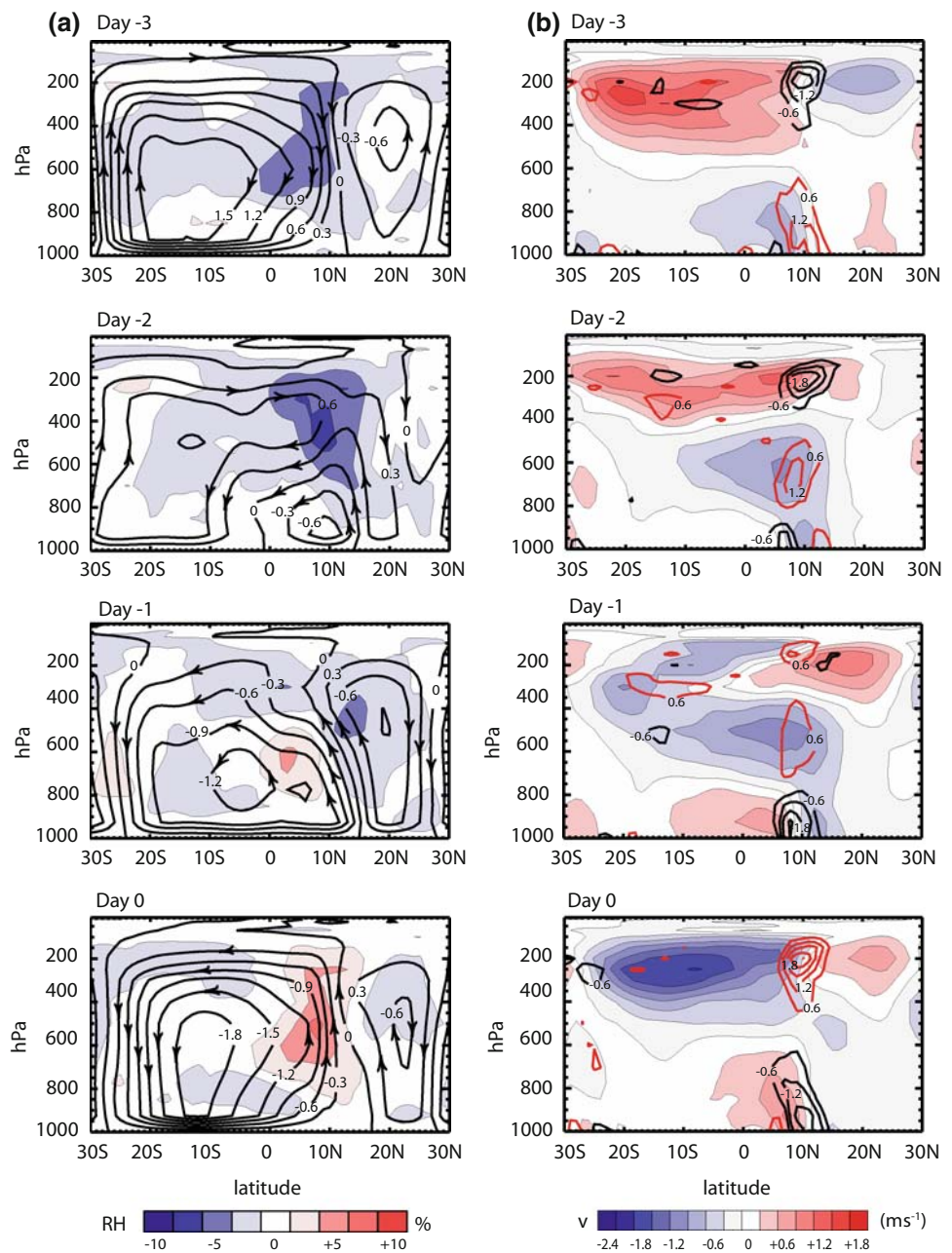
#### 4.2.3 Day –1

Large-scale changes have occurred throughout the domain. The shallow cell has extended into the upper troposphere although remnants still exist but with a weakened southerly flow in the middle troposphere. Relative humidity has started to increase in the middle troposphere equatorward of 10°N. Strong northerly cross-equatorial flow has developed producing strong convergence near 10°N. In the upper troposphere, the flow has become more divergent and cross-equatorial northerly winds have developed.

#### 4.2.4 Day 0

The OLR has reached its most negative value and the anomalous absolute vorticity its most positive. The meridional circulation has increased in magnitude by nearly a factor of two. The relative humidity has increased throughout the near-equatorial northern hemisphere. The lower tropospheric shallow circulation has disappeared entirely and the tropospheric column to the north of the equator is dominated by strong low-level convergence and

**Fig. 8** Composites of the height-latitude circulation between 30°S and 30°N averaged between 120°W and 110°W for day -3 to +3 relative to the occurrence of maximum convection at 10°N. All diagrams are constructed from the 4–8 day band-passed fields. Day 0 of the composites are defined as days in which  $\Delta\text{OLR} \leq 20 \text{ Wm}^{-2}$  at 7.5°N in the 4–8 day band. A total of 40 day 0's were so defined in the June–September period from 1981 to 2000. The figures follow the same format as Fig. 4 with the right-hand panels **a** showing the mass streamfunction ( $10^{11} \text{ kg s}^{-1}$ ) and the relative humidity (%) shaded, bottom scale) and the left-hand panels **b** showing the meridional wind component ( $\text{ms}^{-1}$ , shading, bottom scale) and the horizontal divergence ( $10^{-6} \text{ s}^{-1}$ ). For clarity, we omit zero divergence contour



upper level divergence. The southward cross-equatorial upper-tropospheric flow has reached its strongest magnitude. The low level convergence, near 10°N, strongest at day -1, has weakened and a small region of divergence has developed near 6°N.

#### 4.2.5 Day +1

The overall circulation has weakened by almost 50%. A shallow cell has developed accompanied by strong boundary layer divergence near 6°N and convergence near 700 hPa. A two-cell structure similar to Day -2, although reversed in sign, has developed.

#### 4.2.6 Day +2

The shallow circulation has extended vertically and now occupies the entire troposphere producing anomalous subsidence and drying over the northern hemisphere tropics.

#### 4.2.7 Day +3

The pattern returns to a similar state to that of day -3.

The magnitudes of the band-passed filtered transient anomalies displayed in Fig. 8 are about a factor of two smaller than the mean circulation mass streamfunction

Fig. 8 continued

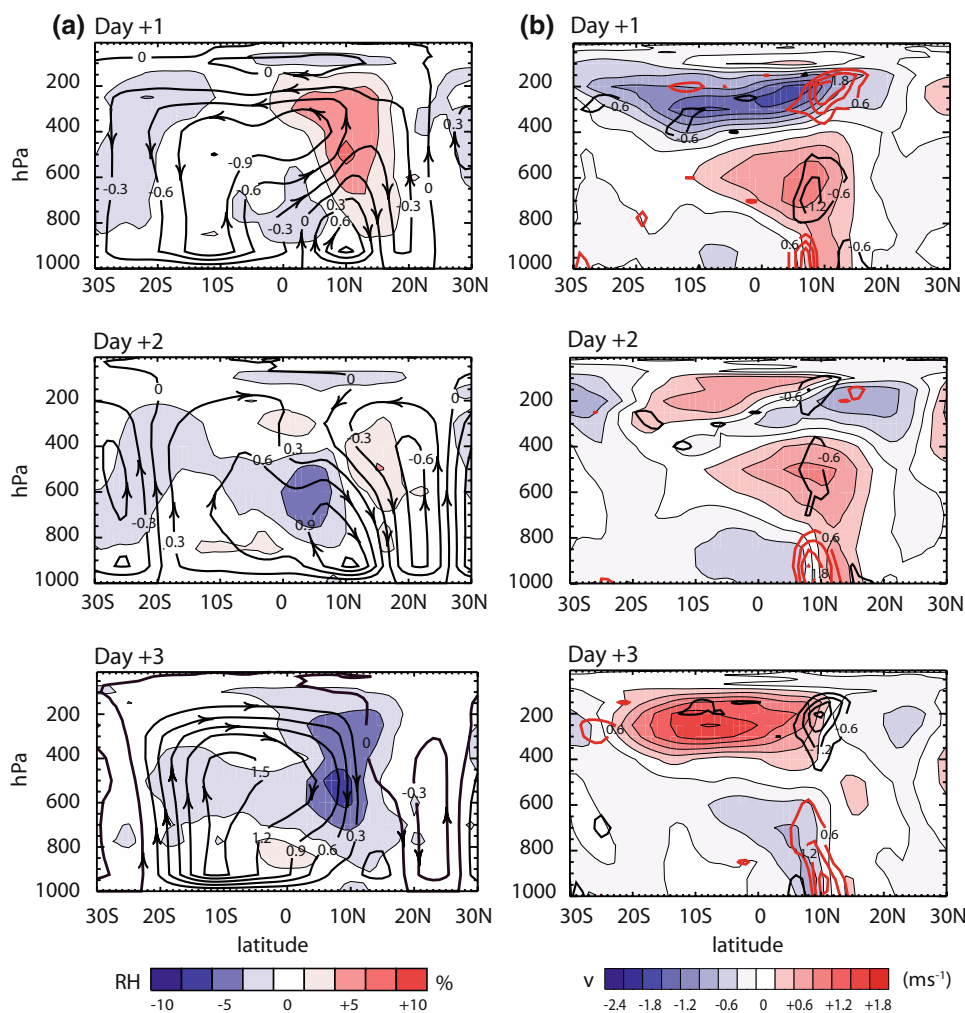


(Fig. 4a). Superimposing the composite circulations on the mean state produces a meridional circulation and convection that oscillates in intensity and also displays a changing latitudinal structure on 4–8 day time scales.

The left hand column of Fig. 9a shows latitude–height distributions of the total circulation (mean plus anomaly) for composite days  $-2$ ,  $0$  and  $+2$ . The right-hand column shows distributions of total heating (the material differential of potential temperature). At all times, the area to the south of the  $\eta = 0$  contour is drier and strongly subsident, leading to efficient radiative cooling in the middle and low troposphere throughout the composite sequence. This cooling lies atop boundary layer heating from the ocean. Over the ocean cool tongue, between  $4^{\circ}\text{S}$  and the equator (see Fig. 1b), there is a narrow band of boundary layer cooling. To the north of  $\eta = 0$  contour, the vertical velocity is positive and moisture extends throughout the entire column. This is a region of intense latent heating that oscillates throughout the composite cycle. During

maximum convective phase (day 0), the latent heating has increased from  $6\text{ K/day}$  at day  $-2$  to  $12\text{ K/day}$  at day 0 at  $500\text{ hPa}$ . The vertical heating structure evolves in a complicated fashion. To examine this behavior, composite time–height distributions of total heating are shown in Fig. 10 for the bands  $10^{\circ}\text{S}–8^{\circ}\text{S}$  and  $8^{\circ}\text{N}–10^{\circ}\text{N}$ . Prior to day 0, the heating is strongest in the lower and middle troposphere. As the convection intensifies, the heating expands upwards forming a new and stronger maximum in the middle upper troposphere. The lower maximum remains and increases in magnitude but does not reach the levels of the more elevated heating maximum.

In summary, the ITCZ oscillates between a highly convective state (day 0) and a period of reduced convection (day  $-3$  or  $+3$ ) cycling through periods of enhanced and reduced heating over the northern hemisphere equatorial regions. The shallow meridional circulation occurring on the transitional days  $-2$  and  $+2$  has many of the characteristics of the ZMB circulation.

**Fig. 9** Height-latitude sections of the total (mean plus anomaly) mass streamfunction ( $10^{11} \text{ kg s}^{-1}$ ) circulations for composite days  $-2, 0$  and  $+2$  (left column). The corresponding height-latitude sections of material tendency of potential temperature  $\theta$  (K/day, gray shading represents positive values) are shown in the right column. **a** Streamfunction and relative humidity. **b** Heating rate

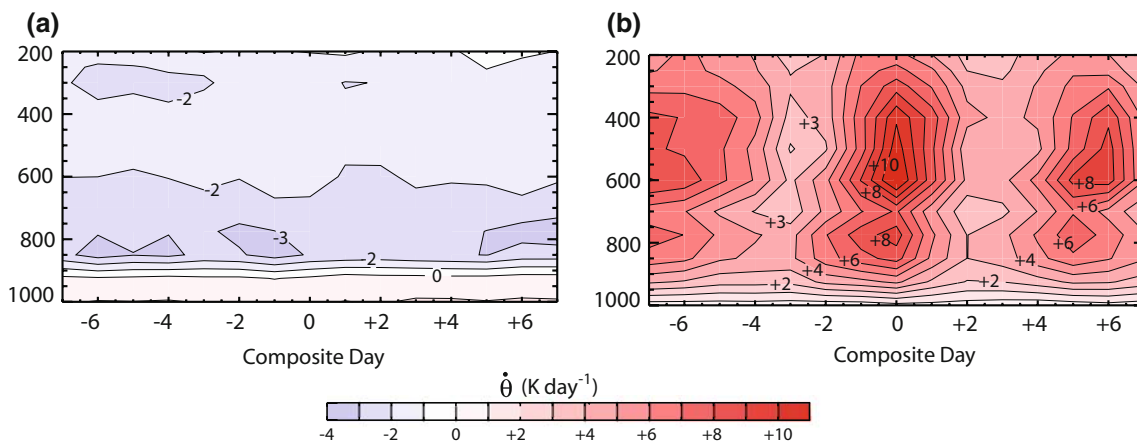
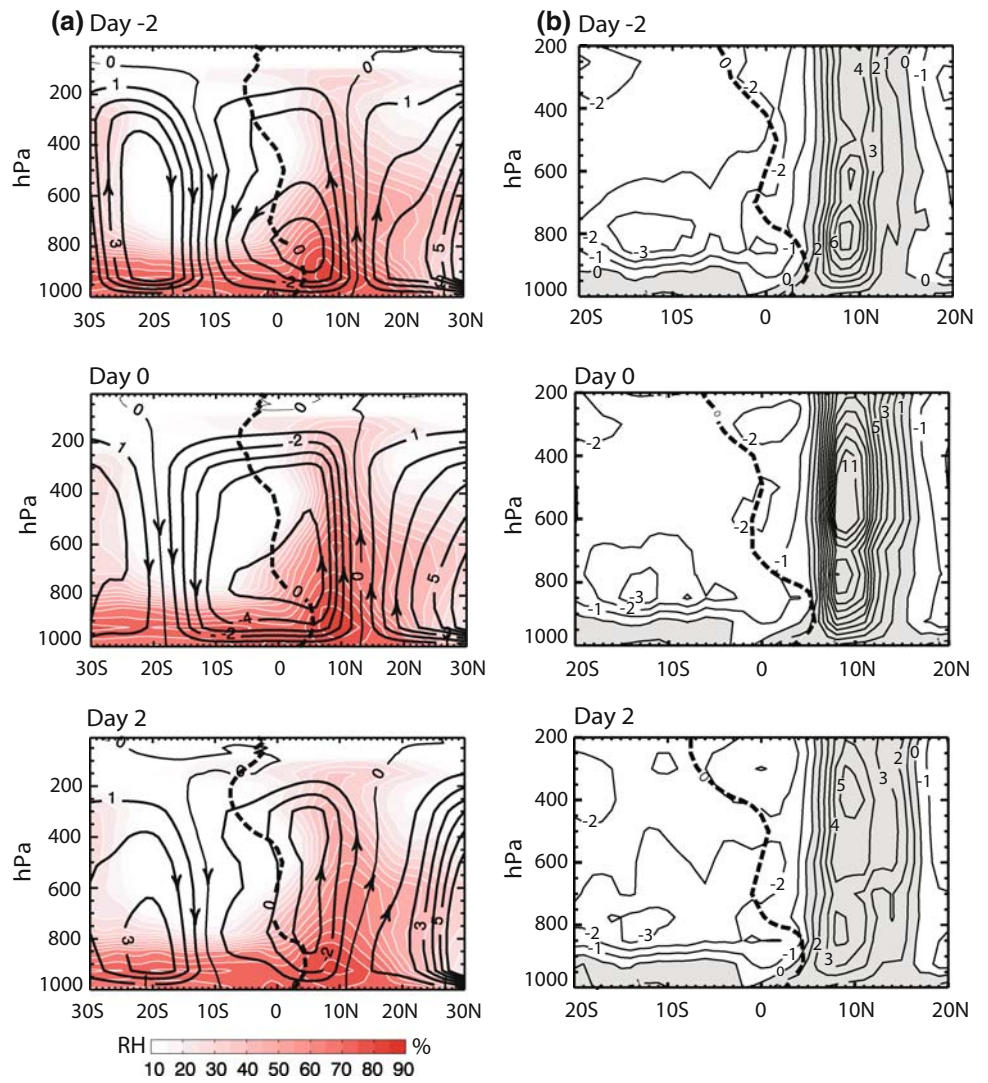


**Fig. 10** Composite day-height sequence of material tendency of the potential temperature  $\dot{\theta}$  (K/day) for two regions. **a**  $120^{\circ}\text{W}$ – $110^{\circ}\text{W}$ ;  $10^{\circ}\text{S}$ – $8^{\circ}\text{S}$  (section A) and **b**  $120^{\circ}\text{W}$ – $110^{\circ}\text{W}$ ;  $8^{\circ}\text{N}$ – $10^{\circ}\text{N}$  (section A), respectively

## 5 Mechanisms

Here we explore the possibility that the oscillations of the ITCZ are driven by regional instabilities. In Part II we will compare this mechanism against the possibility of perturbations being advected from the Atlantic Ocean. The basic hypothesis is that, driven by a finite and negative CEPG, anticyclonic vorticity is advected across the equator rendering the system inertially unstable (e.g., Stevens 1983, TW). However, in a later paper, THW noted that although the circulation signatures appeared to be in agreement with what should be expected in an inertially unstable regime, the linear stability criteria (i.e., an unstable solution for the ageostrophic meridional wind) could only be satisfied in an environment with a cross-equatorial shear far greater than observed. It is important that this issue be resolved. In coming to their conclusions, THW used a well-mixed boundary layer model topped by a temperature inversion ( $\delta\theta = 3^\circ\text{K}$ ) at an altitude of 1–2 km. However, the observed magnitude of the inversion over the warm water north of the equator is less than that used by THW. In an appendix it is shown that in accord with Stevens (1983) and TW that the system is inertially unstable for even relatively small values of cross-equatorial shear. On the basis of the arguments presented in the appendix, we conclude that the linear stability criterion is met for realistic values of stability.

As the CEPG is essentially constant, maintained by the large scale and slowly evolving SST gradient, it may be expected that the system will be in a state of continual forced instability. Analogous situations occur in other parts of the climate system. In the boundary layer during periods of intense solar heating a super-adiabatic lapse rate is maintained and is continually convectively unstable. In attempts to return to stability, turbulent eddies mix heat vertically as long as the surface heating continues. Similarly, the pole-to-equator heating gradient maintains a continual baroclinically unstable state and large scale eddies attempt to return the system to a sub-critical state. Unstable waves will be generated as long as the pole-to-equator temperature is maintained. The composite oscillations shown in Figs. 8 and 9 may be thought of as manifestations of a perpetually unstable system driven by a maintained CEPG. If the location of the mean ITCZ is the result of inertial instability, its location should be predictable by simple theory.

### 5.1 Limits of the mean ITCZ

We have already noted that the region of maximum convergence and convection lies equatorward of the warmest SST and lowest MSLP in regions of strong CEPG (Fig. 2a). Consequently, there must be some counterbalancing

process that retards the northward advance of the anticyclonic vorticity advection. TW and THW speculated that the process must involve the generation of cyclonic vorticity accomplished by vortex tube stretching above the region of convergence on the poleward side of the  $\eta = 0$  contour. Starting with the absolute vorticity equation, we can determine the latitude of maximum convection:

$$\frac{\partial\eta}{\partial t} = -V \cdot \nabla\eta - \eta\nabla \cdot V - \alpha\zeta \quad (1)$$

where  $V$  is the horizontal velocity and  $\alpha$  a dissipation coefficient. In (1), the local tendency of absolute vorticity is determined as the sum of absolute vorticity advection, vortex stretching and dissipation. This equation can be used to help understand basic balances that lead to the circulation differences occurring between the western-central and eastern equatorial Pacific Ocean.

#### 5.1.1 Zero CEPG

With CEPG = 0, the cross-equatorial meridional wind is zero and, hence,  $V \times \nabla\eta = 0$  at the equator. In this circumstance the climatological state is inertially stable with  $\eta > 0$  to the north of the equator and  $\eta < 0$  to the south. Consider the steady state inviscid situation. Within the northern hemisphere, the first two terms on the right-hand side of (1) are capable of making negative contributions. However, in the absence of cross-equatorial advection of absolute vorticity, the first two terms can only contribute to the generation of cyclonic vorticity in the northern hemisphere. The advection term can then only redistribute cyclonic absolute vorticity and the vortex term contributes to a negative tendency if there is divergence. Within this circumstance of zero or small CEPG there are no dynamic controls on the location or intensity of convection. Instead, the location of convection is determined thermodynamically by the SST or dynamically through longitudinal gradients of SST.

#### 5.1.2 Finite CEPG

When a finite CEPG exists, a cross-equatorial flow will be generated flowing down the pressure gradient. When  $V \times \nabla\eta > 0$ , the  $\eta = 0$  contour resides at a finite latitude to the north of the equator. To remain in equilibrium, divergence must occur on the equatorward side of the  $\eta = 0$  contour. This is because  $V > 0$  and  $\nabla\eta > 0$  so that the first term on the right of (1),  $-V \times \nabla\eta < 0$ . Then, for balance (ignoring viscous effects) the second term must be positive: i.e.,  $\eta\nabla \cdot V > 0$ . To the north of  $\eta = 0$ ,  $\eta > 0$  and there must be convergence for balance. As convergence exists in a conditionally unstable atmosphere, deep penetrative convection ensues. These balances explain many of

the circulation characteristics discussed above such as the divergence dipole about the  $\eta = 0$  contour prominent in the mean circulations shown in Figs. 4 and 9 and also in the transient anomaly circulations (Fig. 8). The northward limit of the  $\eta = 0$ , and subsequently the location of convection, can be estimated from the steady state form of (1). In an inviscid system (1) becomes:

$$-V \cdot \nabla V = \eta \nabla \cdot V \tag{2}$$

As latitude increases, the advection term becomes dominated by the advection of planetary vorticity. I.e., with increasing latitude:

$$-V \cdot \nabla \eta \rightarrow -\beta v_d \tag{3}$$

where,  $\beta = df/dy$  and  $v_d$  is the divergent meridional component of velocity forced by the CEPG. Here, following TW, we have taken into account that the velocity vector can be written as the sum of divergent and rotational parts:  $V = V_r + V_d$ . Furthermore, we have noted from Fig. 1c that the pressure gradient is essentially zonal. Thus, the divergent wind vector  $V_d$  is meridional so that  $V_d \approx v_d$ . Furthermore,  $\beta$  is a maximum at the equator and the time averaged derivatives of relative vorticity are small. Thus, (3) is true to good approximation.

Noting that  $\eta = \zeta + f \rightarrow f$  as latitude increases, the right-hand-side of (2) approaches an asymptotic limit for a given divergence. I.e.,

$$\eta \nabla \cdot V \rightarrow f \nabla \cdot V \tag{4}$$

Substituting (3) and (4) into (2) gives:

$$-\beta v_d = f \nabla \cdot V \tag{5}$$

Each term varies with latitude with the left-hand-side varying as  $\cos \phi$  and the right-hand-side as  $\sin \phi$ . Thus, there is only one latitude that will satisfy the equality (5) for a given meridional wind (and hence CEPG) and divergence. Essentially, by controlling the magnitude of the cross-equatorial divergent wind field, the CEPG will determine the latitude of equilibrium. Using (5) to solve for  $\phi_e$ , the latitude of equilibrium, and noting that for small  $\phi_e$ ,  $\tan \phi_e \rightarrow \phi_e$  we obtain:

$$\phi_e \approx v_d / (a \nabla \cdot V) \tag{6}$$

where the divergent meridional wind is given by:

$$v_d = \frac{1}{\alpha} \left( \frac{1}{\rho} \frac{\partial p}{\partial y} - fu \right) \tag{7}$$

where  $\partial p / \rho \partial y = \text{CEPG}$ . Figure 11 shows the equilibrium latitudes as a function of divergent wind speed and divergence. Observed values of 925 hPa divergence and divergent wind region A (see Fig. 9, TW) place the equilibrium latitude between 8 and 10° latitude (shaded region) in the eastern Pacific Ocean. This theoretical estimate matches

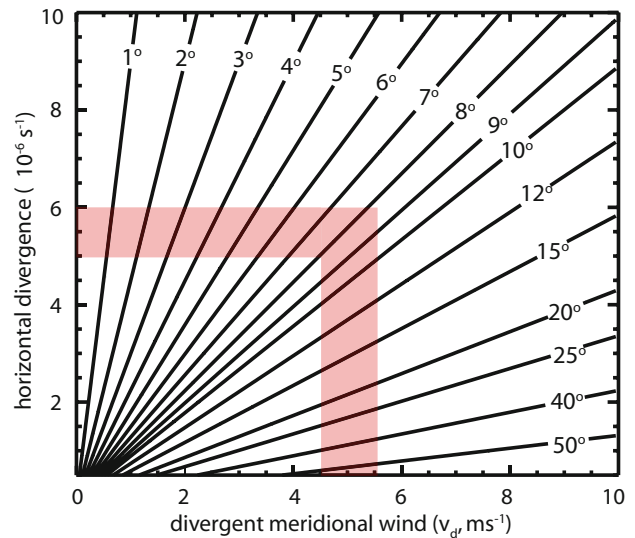


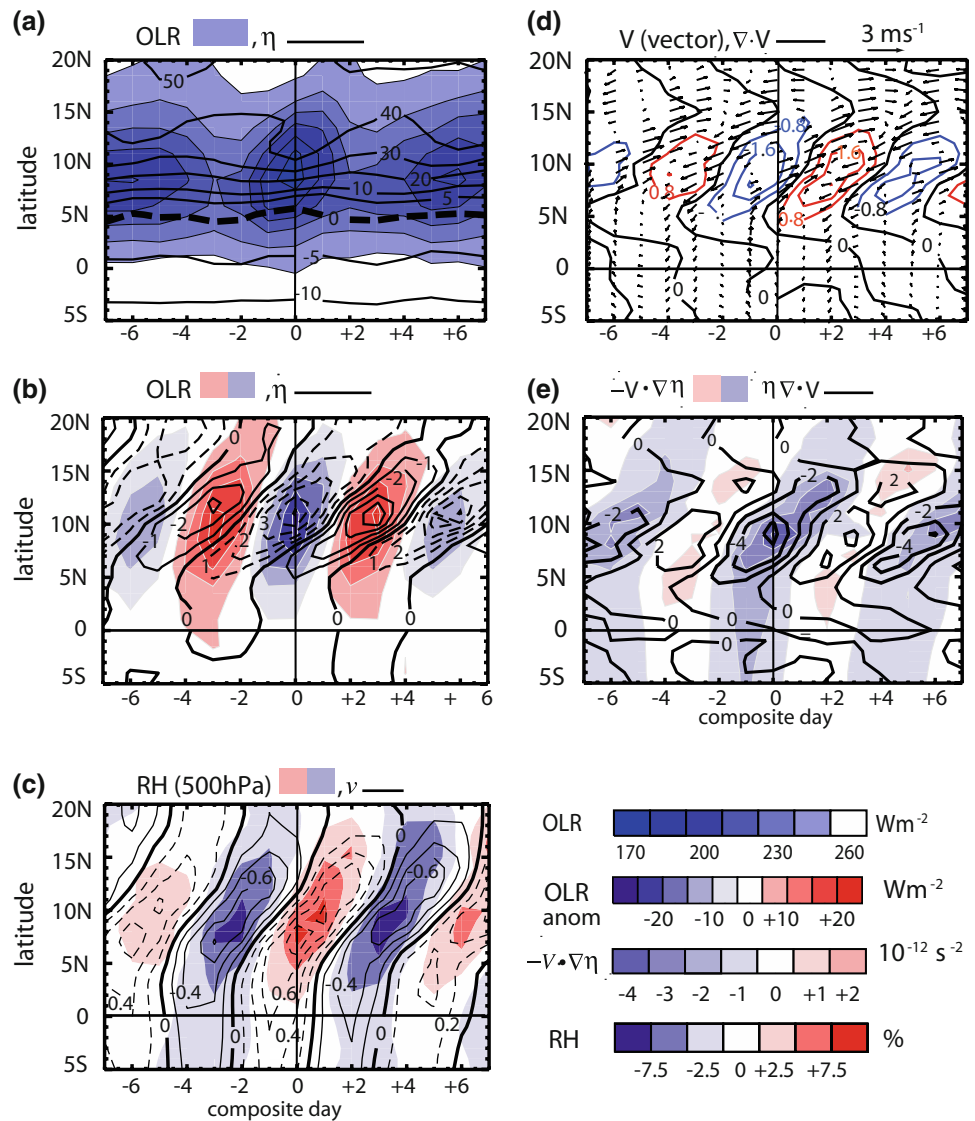
**Fig. 11** Isopleths of the equilibrium latitude,  $\phi_e$ , from (6) as a function of divergence and divergent meridional wind. At these latitudes the advection of negative absolute vorticity equals the generation of cyclonic vorticity by vortex tube stretching. Observed values of the divergent meridional velocity component (from Fig. 9, TW) and divergence at 925 hPa are shown as shaded areas. They intercept near 8–10° latitude matching the observed location of the ITCZ in region A

the observed location of the climatological ITCZ quite well (Fig. 1a).

### 5.2 ITCZ transients

To decipher the physical mechanisms that determine the transient state of the ITCZ, we follow the evolution of the terms in (2). Figure 12 shows of two composite transient cycles (i.e., from day -6 to day +6) as a function of latitude (i.e., from 5°S to 20°N in longitude band A. Panel a shows the evolution of the OLR ( $\text{Wm}^{-2}$ ) and the 925 hPa  $\eta$ -field ( $10^{-6} \text{ s}^{-1}$ ). Against a background of negative OLR, the fields oscillate between deep and shallower convection. Deep convection occurs with the growth of cyclonic absolute vorticity and the extension of the  $\eta = 0$  contour away from the equator. This association is seen more easily in terms of OLR and  $\eta$  anomalies (panel b) except that a strong northward propagation is now apparent. The 925 hPa meridional wind (panel c) shows a clear cross-equatorial flux across the equator at least a day ahead of the OLR maxima anomalies near 10°N. Panel d shows the consistent generation of convergence and divergence ahead of the convective maxima and minima. Finally, panel e shows the evolution of the vortex stretching and divergence terms of the absolute vorticity equation. In the region of

**Fig. 12** Dynamic balances between the transitions of the ITCZ oscillation between composite days  $-6$  to  $+6$ : **a** Time–latitude sequence of the OLR (shaded scale below:  $\text{W m}^{-2}$ ) and the total absolute vorticity at 925 hPa ( $\eta = \zeta + f$ ; contours  $10^{-6} \text{ s}^{-1}$ ); **b** the 925 hPa band-passed absolute vorticity and band-passed OLR (as **a**); **c** the band-passed meridional wind  $v$  (contours  $\text{ms}^{-1}$ ) and 500 hPa relative humidity (shaded bar scale below); **d** the band-passed horizontal velocity vector  $V$  at 925 hPa ( $\text{ms}^{-1}$ , vectors) and 925 hPa divergence ( $\nabla \cdot \vec{V}$ ; contours:  $10^{-6} \text{ s}^{-1}$ ); and **e** absolute vorticity advection ( $-\vec{V} \cdot \nabla \eta$ , shading scale below,  $10^{-12} \text{ s}^{-2}$ ) and vortex stretching term ( $\eta \nabla \cdot \vec{V}$ , contours  $10^{-12} \text{ s}^{-2}$ ) from (3)



maximum convection on day 0, the two terms almost completely balance.

## 6 Summary and conclusions

The mean and transient state of the ITCZ is studied using diagnostic analysis and by the application of some relatively simple dynamics. The results allow us to answer some of the basic questions posed in the introduction.

A major conclusion is that the characteristics of the mean ITCZ may be explained by the atmospheric response to a CEPG, and the divergence and convergence fields that respond to the cross-equatorial advection of anticyclonic vorticity. The CEPG is set up by the large scale and slowly varying SST distribution. The magnitude of the CEPG determines the strength of the divergent wind field and therefore the magnitude of the cross-equatorial vorticity

advection. In turn, convection occurs where convergence is a maximum, just poleward of the  $\eta = 0$  contour. Simple steady state dynamical arguments explain why there is divergence–convergence doublet about the  $\eta = 0$  contour. The latitudinal location of the mean climatological ITCZ (defined here in terms of maximum convection) occurs where the advection of anticyclonic vorticity is balanced by the generation of lower tropospheric vorticity by vortex tube stretching associated with convection. The equilibrium argument allows an estimate of the location of the ITCZ (Eq. 6) that fits well with observations (see Fig. 11).

The character of the dynamical fields at low latitudes agrees well with those expected in an inertially unstable regime as described by Stevens (1983) and TW. However, THW noted that although the system had the appearance of inertially instability, the required basic state would have to be far stronger than observed for the linear stability criterion to be met. We have argued earlier, and at length in the

appendix, that the THW conclusion was based on the assumption of an overly stable layer that does not exist in nature. We conclude that the linear stability criterion is met for realistic values of stability.

The magnitude of the CEPG (Fig. 1c) appears as the discriminating reason for the observed regional differences in the form of the circulations of the ITCZ and the vertical extent of convection. In regions of strong CEPG, maximum convection appears equatorward of the SST maxima and MSLP minima. In regions of small or zero CEPG, the convection is collocated with the extrema of SST and MSLP and there is no dynamic generation of convection to balance a cross-equatorial advection of anticyclonic vorticity. Without dynamic generation of cyclonic vorticity, the convection in the west tends to be weaker than in eastern Pacific. These findings offer some clarity to the dilemma posed by Ramage (1974) and Sadler (1975) regarding the association of convection and SST.

To help describe the nature of the time evolution of the ITCZ, composites of the disturbances were computed. Over a period of 3–6 days, composites show sequentially a build-up of the cross-equatorial advection of anticyclonic vorticity, the build-up of convergence at the latitude of the mean ITCZ, the generation of cyclonic vorticity with increasing deep convection and a retreat of the  $\eta = 0$  contour back towards the equator as cyclonic vorticity is generated in the near-equatorial regions of the northern hemisphere. This process is followed by a further incursion of anticyclonic vorticity as the background CEPG remains essentially unaltered and the dynamic sequence is repeated again and again. The vertical integrated heating in the ITCZ region oscillates between 6 K/day and 12 K/day at the inertial frequency of the location of convection. This latitude is important, as the inertial frequency of this latitude will determine, within this theory, the frequency of the oscillating latent heating. This “inertial oscillator” is the result of a state of continued instability incurred by a very slowly varying CEPG. Figure 3c shows that the time scale of the easterly waves in the eastern Pacific Ocean matches the inertial frequency at the location of the mean ITCZ.

What determines the scale of the forced mode? To date we have argued from a zonally symmetric perspective in essence in a similar manner to Stevens (1983). Bates (1970) found that the fastest growing mode in his zonally symmetric model was 2,000 km, although the basis state in the model did not contain a CEPG. But, in reality, a zonally averaged perspective is not appropriate as the longitudinal scale of the inertial oscillator is finite and is limited by the extent of the finite northward CEPG along the equator as can be seen in Fig. 1c. Westwards of 120°W, the amplitude of CEPG has decreases substantially and the largest magnitudes occur further east. If the CEPG drives the heating variability at the inertial frequency, as described above,

then the scale of the response will be given by the longitudinal scale of the oscillator or roughly 3–4,000 km which approximately matches the wavelength of the easterly waves noted in Fig. 6.

Within the framework of an oscillating ITCZ, the shallow ZMB circulation, apparent in mean meridional circulation shown in Fig. 4a, comes about as a statistical artifact through averaging across the oscillations of the ITCZ. In Fig. 8, the shallow circulation develops on Day -2 to Day -1 before growing in magnitude and extending vertically. The ZMB circulation, as seen in Fig. 4 is representative of the growth of the stabilizing secondary circulation.

The study addressed the very basic question of whether easterly waves (Fig. 6) are the result of the instability mechanism described above, and thus developing in situ in regions of strong CEPG, or the result of waves generated elsewhere and propagating through the eastern Pacific. Here we suggest a very different dynamical circumstance to that offered by Raymond et al. (2006) but one that is supported by the diagnostic work of Serra et al. (2008). Probably, cross-isthmus propagation does occur but here we suggest that local instabilities are a major source of easterly wave activity in the eastern Pacific Ocean.

Given the differences that exist in the literature with regard the source of easterly waves, we consider it prudent to conduct further studies to test the hypothesis that at least a large percentage of waves develop in situ. In Part II, we will show the results of a thorough set of numerical experiments. In these experiments, the initial and boundary conditions were set both to include westward propagating disturbances from the Atlantic Ocean and to exclude them. Both results show in situ formation of waves in the region of strong CEPG of the eastern equatorial Pacific Ocean even in the case where there are no perturbations propagating from the Atlantic. Additionally, it will be shown that the mountains of Central America and Mexico appear not to be a primary reason for easterly wave formation as suggested by Zehnder et al. (1999).

There is a further question that requires investigation. TW noted that there were a number of other regions where the CEPG was appreciable such as the eastern Atlantic Ocean, the northern Indian Ocean in the northern summer and the southern Indian Ocean during the southern summer. In these regions there were ITCZ structures similar to the eastern Pacific Ocean. Are these regions also source regions of waves resulting from inertial instability? Of particular interest is the eastern Atlantic Ocean where, for many years, the Burpee (1972) instability theory has been the accepted theory for the generation of easterly waves. Is an inertial oscillator in the eastern Atlantic also an important source of wave activity?

**Acknowledgments** We would like to acknowledge the late Jim Holton for many stimulating discussions regarding the ITCZ over the years. We are also appreciative of the suggestions made by Dr. J. A. Knox. This research was conducted with funding provided by the Climate Dynamics Division of the National Science Foundation under award NSF-ATM 053177 and NOAA CPPA project NA060OAR4310005.

**Appendix**

We examine the assumptions made by THW in concluding that the linear stability criterion is not met in near equatorial regions of substantial CEPG. In regions where the atmosphere is inertially unstable, the meridional wind accelerates poleward resulting in a divergence–convergence pattern, with divergence equatorward of the zero absolute vorticity line and convergence on the poleward side of  $\eta = 0$  line. However, the effect of the low level horizontal convergence on vertical motion depends on the static stability of the atmosphere. THW assumed a well-mixed boundary layer model topped by a temperature inversion ( $\delta\theta = 3^\circ K$ ) at an altitude of 1–2 km and concluded that the observed zonal wind shear was several time smaller than the shear required to meet the linear instability criterion. To reexamine this issue, we start with the THW model (described in detail in TWH, Sect. 3) that is linearized about a basic zonal wind state:

$$\frac{\partial u}{\partial t} + v \left( \frac{dU}{dy} - \beta y \right) + \alpha u = 0 \tag{8}$$

$$\frac{\partial v}{\partial t} + \beta y u + \frac{\partial \phi}{\partial y} + \alpha v = 0 \tag{9}$$

$$\frac{\partial \phi}{\partial t} + C_B^2 \frac{\partial v}{\partial y} = -\varepsilon \phi \tag{10}$$

where  $u$  and  $v$  represent zonal and meridional wind perturbations,  $\alpha$  is a linear damping coefficient,  $\Phi$  represent the perturbation geopotential, and  $\varepsilon^{-1}$  the boundary layer relaxation time. The parameter  $C_B$  is given by:  $C_B = (gH_B\delta\theta/\theta_0)^{1/2}$ , where  $g$  the gravitational acceleration,  $H_B$  the mean boundary layer depth,  $\delta\theta$  a potential temperature jump at the top of the boundary layer.  $\theta_0$  the reference state potential temperature.

If a constant mean shear is assumed (e.g., Dunkerton 1981) then  $U = \gamma y$ , where  $\gamma$  is a constant of proportionality. Elimination of  $u$  and  $\phi$  from Eq. (8–10) gives:

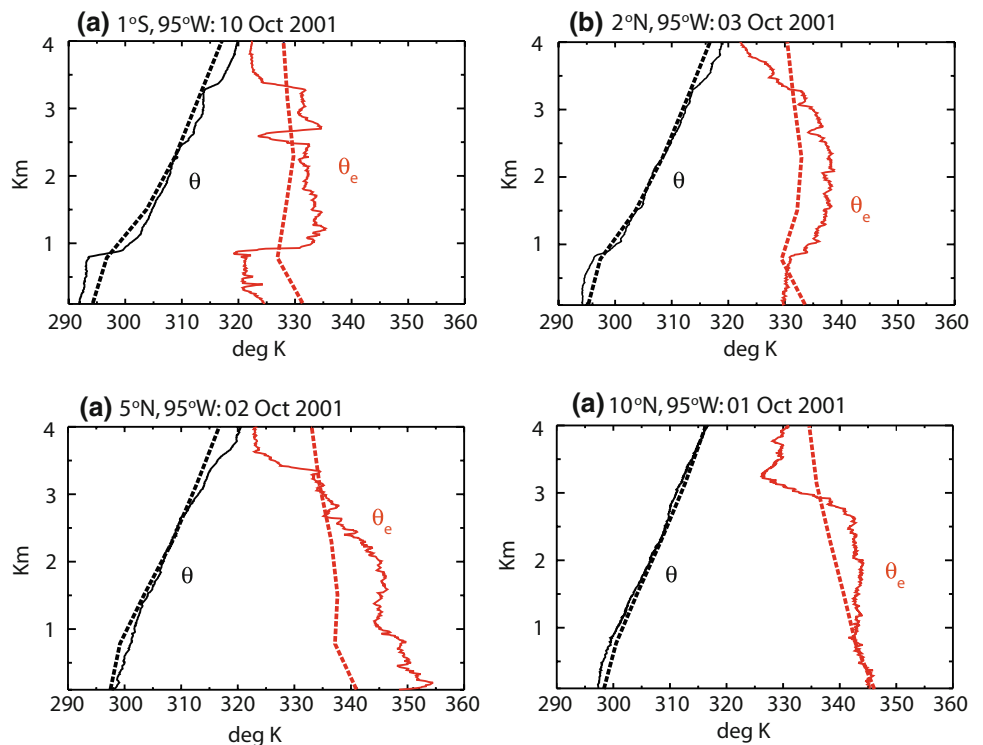
$$\left( \frac{\partial}{\partial t} + \alpha \right)^2 v + (\beta y(\beta y - \gamma))v - C_B^2 \frac{\partial^2 v}{\partial y^2} = 0 \tag{11}$$

Assuming an exponential form for  $v$ :

$$v(y, t) = V(y)e^{i\omega t}, \tag{12}$$

a solution with the form  $V(y) = V_0 \exp(-v^*y/2)$  has been found, where  $v^* = (\beta/C_B)^{1/2}y$  which possess eigenvalues:

**Fig. 13** Vertical profiles of potential temperature (black) and equivalent potential temperature (red) for the eastern Pacific ITCZ during 1–10 October, 2001 period using atmospheric soundings from the NOAA ship Ron Brown cruise in support of the Eastern Pacific Investigations of Climate (EPIC) field campaign (thick line). For comparison, long term mean (1981–2000) profiles for July (dotted lines) were calculated using the ERA 40 dataset



$$(\omega - i\alpha)^2 + \frac{\gamma^2}{4} = \beta C_B \quad (13)$$

Equation 13 shows that instability (i.e.,  $\omega$  imaginary) occurs only if the linear shear of the zonal wind ( $\gamma$ ) is greater than a critical value:  $\gamma^2 > 4\beta C_B$ . THW calculated that for inertial instability to occur with  $H_B \sim 1$  km and a potential temperature jump ( $\delta\theta$ ) of 3°K, the flow speed must increase by more than 30 ms<sup>-1</sup> over 10° latitude. However, for much smaller values of potential temperature jump (i.e., a reduced cap at the top of the boundary layer) instability can occur for much smaller value of shear of the zonal wind. This turns out to be the case for the eastern Pacific Ocean.

Figure 13 shows the vertical profile of potential temperature and equivalent potential temperature obtained from atmospheric soundings launched from the NOAA Research Ship *Ron Brown* cruise (thick line) during the East Pacific Investigation of Climate (EPIC) 2001 field campaign (Raymond et al. 2004). Analyses close to 1800 UTC are presented for 1°S, 2°N, 5°N, and 8°N, and 95°W. The character of the atmospheric boundary layer changes from equator to the north, with very distinct profiles of potential temperature. While at 1°S and 2°N there is an apparent cap at the top of the atmospheric boundary layer ( $\delta\theta = 3^\circ - 6^\circ\text{K}$ ), at 5°N and 8°N the atmosphere seems to be at least neutrally stratified with no stable cap at the top of the boundary layer. The data used in Fig. 13 is similar to the EPIC 2001 NCAR C-130 research aircraft dropwindsondes (deSzoeko et al. 2005). When moisture is considered, it is apparent from both Fig. 13c and d that the more northward profiles (5°N and 8°N) are conditionally unstable. For comparisons, long-term mean (1981–2000) potential temperature and equivalent potential temperature profiles for July, were calculated using the ERA 40 reanalysis dataset. A similar vertical structure of both potential temperature and equivalent potential temperature was found. Thus, the conclusions made by THW do not hold for the northern regions (5°N and 8°N) and, for values of  $\delta\theta \approx 0$ , the linear criterion for inertial instability is met for any shear of the zonal wind  $\gamma > 0$ .

## References

- Bates JR (1970) Dynamics of disturbances on the intertropical convergence zone. *Q J R Meteorol Soc* 96:677–701. doi:[10.1002/qj.49709641010](https://doi.org/10.1002/qj.49709641010)
- Biasutti M, Battisti DS, Sarachik ES (2003) The annual cycle over the tropical Atlantic, South America, and Africa. *J Clim* 16(15): 2491–2508. doi:[10.1175/1520-0442\(2003\)016<2491:TACOTT>2.0.CO;2](https://doi.org/10.1175/1520-0442(2003)016<2491:TACOTT>2.0.CO;2)
- Burpee RW (1972) The origin and structure of easterly waves in the lower troposphere of North America. *J Atmos Sci* 29:77–90. doi:[10.1175/1520-0469\(1972\)029<0077:TOASOE>2.0.CO;2](https://doi.org/10.1175/1520-0469(1972)029<0077:TOASOE>2.0.CO;2)
- Chang CP (1970) Westward propagating cloud patterns in the tropical Pacific as seen from time-composite satellite photos. *J Atmos Sci* 27:133–138. doi:[10.1175/1520-0469\(1970\)027<0133:WPCPIT>2.0.CO;2](https://doi.org/10.1175/1520-0469(1970)027<0133:WPCPIT>2.0.CO;2)
- deSzoeko SP, Bretherton CS, Bond NA, Cronin MF, Morely BM (2005) EPIC 95°W observations of the eastern Pacific atmospheric boundary layer from the cold tongue to the ITCZ. *J Atmos Sci* 62(2):426
- Dunkerton TJ (1981) On the inertial instability of the equatorial middle atmosphere. *J Atmos Sci* 38:2354–2364
- Farlan LM, Zehnder JA (1997) The interaction of easterly waves, orography, and the intertropical convergence zone in the genesis of eastern Pacific tropical cyclones. *Mon Weather Rev* 125:2683–2698
- Ferreira RN, Schubert WH (1997) Barotropic aspects of ITCZ. *J Atmos Sci* 54:261–285
- Frank NL (1970) Atlantic tropical systems of 1969. *Mon Weather Rev* 98:307–314
- Grist JP, Nicholson SE (2001) A study of the dynamic factors influencing the interannual variability of rainfall in the West African Sahel. *J Clim* 14:1337–1359
- Hastenrath S, Lamb PJ (1977a) Climate atlas of the tropical Atlantic and eastern Pacific oceans. University of Wisconsin Press, Wisconsin, p 112
- Hastenrath S, Lamb PJ (1977b) Some aspects of circulation and climate over the eastern Atlantic. *Mon Weather Rev* 106:1280–1287
- Holton JR, Wallace JM, Young JA (1971) On boundary layer dynamics and the ITCZ. *J Atmos Sci* 28:180–275
- Lindzen RS, Nigam S (1987) On the role of sea surface temperature gradients in forcing low level winds and convergence in the tropics. *J Atmos Sci* 44:2418–2436
- Nicholson SE, Webster PJ (2007) A physical basis for the interannual variability of rainfall in the Sahel. *Q J R Meteorol Soc* 133:2065–2084
- Palmer CE (1952) Tropical meteorology. *Q J Roy Met Soc* 78:126–164
- Ramage CS (1974) Structure of an oceanic near-equatorial trough deduced from research aircraft traverses. *Mon Weather Rev* 102:754–759
- Raymond DJ, Esbensen SK, Paulson C, Gregg M, Bretherton CS, Petersen WA, Cifelli R, Shay LK, Ohlmann C, Zuidema P (2004) EPIC2001 and the coupled ocean–atmosphere system of the tropical east Pacific. *Bull Am Meteorol Soc* 85(9):1341–1354
- Raymond DJ, Bretherton CS, Molinari J (2006) Dynamics of the intertropical convergence zone of the East Pacific. *J Atmos Sci* 63:582–597
- Reynolds RW, Rayner NA, Smith TM, Stokes DC, Wang WQ (2002) An improved in situ and satellite SST analysis for climate. *J Clim* 15:1609–1625
- Riehl H (1945) Waves in the easterlies and the polar front in the tropics. Misc. Rept. No. 17. Department of Meteorology, University of Chicago, Chicago
- Sadler JC (1975) The monsoon circulation and cloudiness over the GATE area. *Mon Weather Rev* 103:369–387
- Serra YL, Kiladis GN, Cronin MF (2008) Horizontal and vertical structure of easterly waves in the Pacific ITCZ. *J Atmos Sci* 65:1266–1284
- Serra YL, Kiladis GN, Hughes KI (2009) Easterly waves over the Intra-American Sea region. *J Clim* (in press)
- Stevens D (1983) On symmetric stability and instability of zonal mean flows near the equator. *J Atmos Sci* 40:882–893
- Thornicroft CD, Hoskins BJ (1994) An idealized study of African easterly waves. I: A linear view. *Q J Roy Met Soc* 120:953–982
- Toma VE, Webster PJ (2008) Oscillations of the Intertropical Convergence Zone and the genesis of easterly waves. Part II: Numerical experiments. Submitted to *Clim. Dyn*

- Tomas R, Webster PJ (1997) On the location of the Intertropical Convergence zone and near-equatorial convection: The role of inertial instability. *Quar J Roy Met Soc* 123:1445–1482
- Tomas RA, Holton JR, Webster PJ (1999) The influence of cross-equatorial pressure gradients on the location of near-equatorial convection. *Q J Roy Met Soc* 125:1107–1127
- Uppala SM, Kållberg PW, Simmons AJ, Andrae U, da Costa Bechtold V, Fiorino M, Gibson JK, Haseler J, Hernandez A, Kelly GA, and 35 coauthors (2005) The ERA-40 reanalysis. *Q J Roy Met Soc* 131:2961–3012
- Waliser DE, Somerville RCJ (1994) Preferred latitudes of the intertropical convergence zone. *J Atmos Sci* 51:1619–1639
- Wang CC, Magnusdottir G (2005) ITCZ breakdown in three-dimensional flows. *J Atmos Sci* 62:1497–1512
- Webster PJ, Lukas R (1992) TOGA-COARE: the coupled ocean–atmosphere response experiment. *Bull Amer Met Soc* 73:1377–1416
- Yanai MT, Maruyama T, Nitta Y, Hayashi (1968) Power spectra of large scale disturbances over the tropical Pacific. *J Met Soc Jpn* 46:308–323
- Zehnder JA, Powell DM, Ropp DL (1999) The interaction of easterly waves, orography, and the intertropical convergence zone in the genesis of eastern pacific tropical cyclones. *Mon Weather Rev* 127:1566–1585
- Zhang C, McGauley M, Bond NA (2004) Shallow meridional circulation in the tropical eastern Pacific. *J Clim* 17:133–139